Electron Paramagnetic Resonance Study of Radiation Damage in Photosynthetic Reaction Center Crystals[†]

Lisa M. Utschig, Sergey D. Chemerisov, David M. Tiede, and Oleg G. Poluektov*

Chemical Sciences and Engineering Division, Argonne National Laboratory, 9700 South Cass Avenue, Argonne, Illinois 60439

Received April 2, 2008; Revised Manuscript Received July 11, 2008

ABSTRACT: Electron paramagnetic resonance (EPR) was used to simultaneously study radiation-induced cofactor reduction and damaging radical formation in single crystals of the bacterial reaction center (RC). Crystals of Fe-removed/Zn-replaced RC protein from *Rhodobacter* (*R.*) *sphaeroides* R26 were irradiated with varied radiation doses at cryogenic temperature and analyzed for radiation-induced free radical formation and alteration of light-induced photosynthetic electron transfer activity using high-field (HF) D-band (130 GHz) and X-band (9.5 GHz) EPR spectroscopies. These analyses show that the formation of radiation-induced free radicals saturated at doses 1 order of magnitude smaller than the amount of radiation at which protein crystals lose their diffraction quality, while light-induced RC activity was found to be lost at radiation doses at least 1 order of magnitude lower than the dose at which radiation-induced radicals exhibited saturation. HF D-band EPR spectra provide direct evidence for radiation-induced reduction of the quinones and possibly other cofactors. These results demonstrate that substantial radiation damage is likely to have occurred during X-ray diffraction data collection used for photosynthetic RC structure determination. Thus, both radiation-induced loss of photochemical activity in RC crystals and reduction of the quinones are important factors that must be considered when correlating spectroscopic and crystallographic measurements of quinone site structures.

X-ray crystallography is a central tool for the determination of macromolecular protein structures; yet synchrotron radiation-induced effects to crystals remain a major concern for protein crystallographers. X-ray radiation-induced free radical formation and subsequent bond breakage and cofactor oxidation state changes could result in modifications that alter the native activity of the protein, with the resultant protein structure reflecting a nonfunctional state. These concerns are particularly significant for proteins containing catalytic metal centers or redox-active cofactors (*1*−*6*). For example, an X-ray absorption spectroscopic (XAS)[1] study of the Mn_4Ca oxygen evolving complex in photosystem II (PSII) RC crystals showed significant X-ray induced oxidation state and structural changes to the metal cluster under radiation exposure conditions typically used for obtaining crystallographic data (*7*). Unlike XAS studies, wherein only metal site changes are observable, electron paramagnetic resonance (EPR) provides a means to look at radiation-induced radical formation in the entire protein. The photosynthetic bacterial reaction center (RC) (*8, 9*) is an excellent system for studying the effects of radiation, as the protein contains several potential radiation-reducible redox-active cofactors whose radical formation can be directly monitored spectroscopically after radiation exposure. We have applied EPR spectroscopy to directly investigate the consequences of radiation on photosynthetic function of the RC, an integral membrane protein that converts light energy into chemical energy (*10, 11*).

In the RC, sequential electron transfer occurs following photoexcitation of a special pair of bacteriochlorophylls, P, through a series of acceptors, terminating in the electron transfer between two quinones, Q_A and Q_B. Q_B functions as a two-electron, two-proton acceptor following successive turnovers of RC photochemistry (*12*). $Q_A^-Q_B \rightarrow Q_AQ_B^-$ electron transfer is a temperature-activated (*13, 14*), conformationally gated reaction (*15*), and the dynamic, functional positioning of Q_B as well as the nature of the conformational gate has been the subject of much debate.

Several crystallographic studies of the *Rhodobacter sphaeroides* RC have focused on the location of Q_B (*9, 16*−*20*), yet no consensus about the functional relevance of the multiple structurally determined quinone binding sites has been achieved. Two distinct sites of Q_B, the "distal" and "proximal" positions, have been observed in *R. sphaeroides* RC crystal structures, and movement of Q_B between these two positions has been proposed to represent the conformational gate for the interquinone electron transfer reaction (*16*). Recent cryogenic crystallographic studies have confirmed a distributed occupancy of the Q_B cofactor between distal and proximal sites but have shown that the distribution between the two sites is comparable in both light and dark structures and is possibly modulated by pH (*18, 21*).

In contrast to crystallographic studies that show a multiplicity of Q_B binding sites and possible light-induced shifts between them, spectroscopic studies of RCs in noncrystalline state, including FTIR and optical measurements, have argued

[†] This work was supported by the U.S. Department of Energy, Office of Basic Energy Sciences, Division of Chemical Sciences, Geosciences, and Biosciences, under Contract DE-AC02-06CH11357.

* To whom correspondence should be addressed. Phone: (630) 252-3546. Fax: (630) 252-9289. oleg@anl.gov.

[1] Abbreviations: EPR, electron paramagnetic resonance; RC, reaction center; *R.*, *Rhodobacter*; HF, high field; XAS, X-ray absorption spectroscopy; PSII, photosystem II; UV, ultraviolet; IR, infrared.

10.1021/bi800574e CCC: $40.75
Published on Web 08/09/2008

against a large-scale, light-induced shift in the position of Q_B as a part of the first electron transfer gating mechanism for RCs (*22*−*24*). Furthermore, high-field (HF) EPR experiments have shown that no reorientation of Q_B^- or structural changes in the protein environment near Q_B are observed for distinct kinetic states of electron transfer (*25*). Questions concerning the native position of the primary quinone acceptor are also evident from spectroscopic studies. Analyses of recent HF time-resolved EPR spectroscopic results suggest that the orientation of Q_A^- is different than that of Q_A determined from X-ray crystal structures (*26, 27*). Like Q_B, the reduction state of Q_A and the ability of Q_A to accept light-induced electrons are not known following X-ray irradiation. The possibility of radiation damage to the protein complicates correlation of X-ray data with details of light-induced RC function.

Herein, we report the first EPR study of radiation-induced effects in a photosynthetic RC crystal. One advantage of using EPR is that the concomitant appearance of radiation damage and loss of protein function at specific radiation doses can be measured. The enhanced spectral resolution of HF EPR allows complete resolution of the *g*-tensor components of the radical species involved in light-induced electron transfer (*28, 29*), and radiation-induced reduction or oxidation of cofactors would be discernible with HF EPR. However, in order to see resolved P^+, Q_A^-, and Q_B^- signals with D-band (130 GHz/4.6 T) EPR, the non-heme Fe^{2+} in RCs that is magnetically coupled to the quinones must be removed and replaced with diamagnetic Zn^{2+} (*25, 30*). Thus, to investigate radiation effects we have prepared the first crystals of biochemically Fe-removed/Zn-replaced RCs and have developed methods for radiating and freeze-trapping these single crystals for cryogenic EPR measurement of radiation-induced radical species. These experiments provide insight into the effects of X-ray data collection on redox cofactor structure and photosynthetic function and show that loss of protein light activity and substantial radiation damage occur at significantly lower doses than reported values of radiation at which protein crystals lose their diffraction quality.

MATERIALS AND METHODS

Protein Preparation and Crystallization. The non-heme Fe^{2+} in RCs is magnetically coupled to the quinones, giving rise to a broad $[Fe^{2+}Q_A]^-$ EPR resonance centered at $g \sim 1.8$. In the absence of paramagnetic metal, the quinone EPR signal narrows to that of a typical organic radical with $g_{av} = 2.0045$ and at high magnetic field can be resolved from the P^+ EPR signal. Zn^{2+} was substituted into the Fe site using a modification to the procedure of Utschig (*30*), as recently reported (*25*). To our knowledge, this is the first report of the crystallization of biochemically Zn-replaced RCs. Whereas biosynthetically prepared Zn-RCs contain ~30% Zn (*31*), biochemical replacement routinely yields >80% Zn incorporation (*25, 30*).

Purified protonated RCs from *R. sphaeroides* R26 ($OD_{803} \sim 25\ cm^{-1}$ in 10 mM Tris-HCl, pH 7.8, 10 μM EDTA, 280 mM NaCl, and 0.045% LDAO) with 2 mM *o*-phenanthroline and 0.9−0.95 M LiSCN were placed on ice. After 30 min, 1 mM $ZnSO_4$ and 9 mM 2-mercaptoethanol were added, and the solution was incubated an additional 30 min. LiSCN was removed by overnight (>18 h) dialysis against 10 mM Tris-HCl, pH 7.8, 10 μM EDTA, 280 mM NaCl, 0.045% LDAO, and 6 g of Chelex 100 metal-chelating resin (Bio-Rad), with two buffer changes. Four mol equiv of protonated ubiquinone-10 from a 2.7 mM stock solution (1% LDAO) was heated at 65 °C for 5 min for quinone solubilization. The quinone/RC mixture was incubated for 30 min. This procedure results in a high percentage of quinone incorporation at both Q_A and Q_B sites (*25*). Samples were concentrated with microcon-50 ultrafiltration devices (Amicon) to 22−30 mg/mL for crystallization setup. Metal ion content was determined as described previously (*30*).

Crystallization conditions were based on the procedure of Pokkuluri (*32*) with slight modifications. Equal parts of a concentrated RC solution and phosphate buffer (1.6 M potassium phosphate, pH 7.5, 6.5% hexanetriol, and 4.0% dioxane) were combined, and 25 μL of this solution was used as sitting vapor diffusion droplets. The RC mixture was equilibrated (at 22 °C) against a 1 mL reservoir of 1.6 M phosphate, pH 7.5, in the dark. The first appearance of crystals took at least 6 weeks. Rectangular prism-shaped single crystals (0.2−1 mm size) were placed in either 4 mm o.d. X-band or 600 μm o.d. D-band quartz EPR tubes, and the tube ends were sealed.

Crystal Irradiation. A van de Graaff accelerator was used to irradiate the RC crystals. An electron beam (e-beam) and X-ray induce similar radiation effects that result in identical types of radiation damage. Both e-beam and X-ray radiation produce secondary electrons which deposit energy by creating small spurs (or clusters) of excited and ionized species. The chemistry that results from these spurs accounts for the majority of radiation-induced processes (i.e., bond breaking, reduction, recombination) (*33, 34*). Thus, the degree of radiation damage is not dependent on the source of radiation and can be directly correlated to the amount of deposited energy or dose of radiation. The use of electron irradiation instead of X-ray irradiation was chosen primarily to simplify sample handling and to shorten the accumulation time needed to reach the required radiation doses. In the case of an e-beam, irradiation can be done directly in EPR quartz tubes that have a wall thickness of 500 μm. Such direct irradiation is not possible with an X-ray beam due to the high absorption of X-rays by quartz. Furthermore, irradiation with an e-beam allows for easy transfer of the sample from the irradiation facility to the EPR spectrometer without warming the protein crystal.

Multiple crystal samples were used for these experiments; each individual crystal was handled as detailed. For X-band measurements, a single RC crystal was transferred into a precooled 4 mm o.d. quartz EPR tube and then evacuated and sealed. For D-band experiments, a D-band (o.d. 600 μm) EPR tube containing a single RC crystal was placed in a 4 mm o.d. quartz EPR tube. The crystals were irradiated at 77 K with a 3 MeV e-beam from the van de Graaff accelerator. Temperature was controlled by continuously spraying liquid nitrogen on the EPR tube during irradiation. To avoid the large EPR signal that is formed in irradiated quartz, the 4 mm tube was inverted during removal from the liquid nitrogen stream and plunged into a dewar of liquid nitrogen for transport to the EPR spectrometer. D-band tubes were dropped from the 4 mm EPR tubes directly into a pool of liquid nitrogen prior to insertion into the precooled D-band cavity.

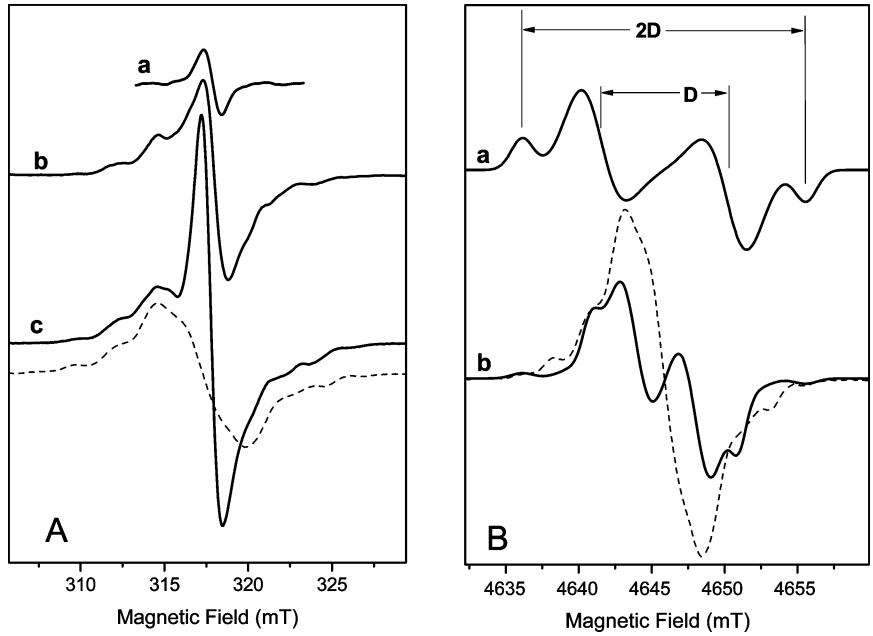

FIGURE 1: (A) X-band (9.5 GHz) EPR spectra recorded after different doses of radiation: (a) 0.03 MGy; (b) 0.38 MGy; (c) 2 MGy. For comparison, a D-band (130 GHz) EPR spectrum recorded at the radiation dose of 2 MGy is shown as a dashed line. (In order to overlay the spectra, the D-band spectrum was replotted using the X-band resonance field; the magnetic sweep range was unchanged.) (B) Theoretically simulated D-band EPR spectra. (a) Spectrum of the radical with a zero-field splitting parameter $D = 97$ G, which corresponds to a distance of 6.7 Å between radicals. (b) Sum of two theoretically simulated spectra of radical pairs (corresponding to distances of 6.7 and 8 Å) that demonstrates how the experimental D-band EPR spectrum (radiation dose of 2 MGy, shown as dashed line) can be built from a number of radical pair spectra.

EPR Spectroscopy. X-band (9.5 GHz) EPR measurements were carried out with a Bruker Elexsys E580 spectrometer (Bruker Biospin Corp.) equipped with a standard rectangular cavity. HF EPR measurements were performed on a home-built pulsed/continuous wave D-band (130 GHz) EPR spectrometer, as described previously (*35*), equipped with a single mode cylindrical cavity TE_{011}. Samples were transferred from liquid nitrogen to precooled microwave cavities at 4 K (X-band) or 10 K (D-band). The temperature was controlled with an Air Products (X-band) or Oxford (D-band) temperature control system. To measure light-induced protein activity, X-band EPR spectra were recorded at 4 K under continuous illumination with a 300 W Xe lamp (ILC). A 400 nm cutoff filter was used to remove photons from the UV spectral region, and a water filter (15 cm length) was used to remove the IR contribution.

Dose Calculation. Dose calculations were conducted using an electron gamma shower (EGSnrc) (*36*) computer code. Electron flux of the 3 MeV electrons from the Van de Graaff accelerator through the 6 mm diameter aperture was measured using a Faraday cup, and this number was used for the calculations. The dose rate that results from these calculations is 33 Gy per 100 nC electron pulse or 330 Gy/s for 10 Hz repetition rate used in the experiment.

RESULTS AND DISCUSSION

The questions addressed herein concern the damage and cofactor redox state changes that result from radiation exposure to RC crystals during X-ray data collection and how these effects potentially impact the interpretation of structural details from crystal structures in terms of functional significance. Our multifrequency EPR study provides new information about the nature of the radiation-induced free radical damage in RC crystals, the corresponding changes in light-induced photosynthetic function, and the dose dependencies at which these effects occur. To the best of our knowledge, this is the first time that HF EPR has been used to characterize the free radical products of exposure of a biomolecule to ionizing radiation.

EPR spectra of irradiated RC single crystals show that, at cryogenic temperatures, radiation exposure leads to the creation of a variety of free radicals within the RC protein environment. The nature of the radical species created in biopolymers upon irradiation has been a subject of numerous studies (*2, 4, 37*−*42*). Direct radiation-induced bond breakage has been associated with the formation of spin-coupled radical pairs that are held at fixed distances (*43*−*45*). In addition, a range of isolated free radical species are generated by radiation exposure. EPR studies of proteins have shown direct radiation damage of the amide backbone (*38*) and the migration of the solvated electron through large distances along the peptide backbone before being trapped at specific sites (*4*). Sites for damage accumulation include disulfide bonds and aspartate, glutamate, tyrosine, and methionine residues (*2, 4, 39*−*41*). Protein cofactors are also candidate sites for solvated electron and free radical trapping. In the RC, cofactor sites include the π-radical forming bacteriochlorophyll, bacteriopheophytin, and quinone groups (*10, 11*). The advantage of HF EPR is that it offers the opportunity to resolve sites of radiation-induced free radical accumulation by resolution of molecular group specific g-tensors and to distinguish between protein and cofactor trapping sites.

Figure 1A shows X-band EPR spectra of Fe-removed/Zn-replaced RC crystals measured following radiation exposure at 77 K with doses 0.03, 0.38, and 2 MGy, displayed in traces labeled a thru c, respectively. A composite signal is seen to grow in with increasing radiation dose. This signal is composed of a central free radical signal flanked by high-

and low-field tails that have a pattern of partially resolved peaks. The partially resolved, split peak pattern is characteristic of spectra associated with radical pairs in which the two radicals are separated by a fixed distance (*43*−*45*). This assignment can be confirmed by recording HF D-band spectra. Structured EPR absorption associated with Zeeman interactions within the EPR Hamiltonian will be shifted by recording spectra at higher frequency, while splitting resulting from spin−spin interactions will be frequency independent (*46*). On Figure 1A a HF D-band EPR spectrum, measured following a 2 MGy dose exposure, is plotted for comparison to the corresponding X-band EPR spectrum. The D-band spectrum shows a broadening of the central free radical signals associated with frequency-dependent Zeeman broadening. The structure of the spectral tails is frequency-independent.

An analysis of the radical pair EPR signals is shown in Figure 1B. Electron spin dipole−dipole interaction leads to splitting of the EPR spectra. This dipole−dipole interaction is characterized by the zero-field splitting parameter D and can be extracted from the EPR spectra, as shown in Figure 1B (a). In the simplest model of the point-dipole approximation, the D-parameter allows for estimation of distances between radicals according to the expression $D = (3g\beta_e)/(4r^3)$, where g is the radical g-value, β_e is the Bohr magneton, and r is the distance between spins in a radical pair. The simulated spectrum shown in Figure 1B (b) demonstrates how the broadened splittings observed in the experimental spectrum can result from overlapping spectra of radical pairs having a distribution of separation distances. Note that distinct peaks in the spectrum of radical pairs indicate that the radicals are being held at fixed positions within the RC structure. Furthermore, the radical pair separations are found to be clustered around a discrete set of distances that are largely uniform throughout the crystal sample and are retained during the accumulated radiation dose at low temperature. These discrete distances are 6.3, 7, and 8 Å, as determined from the pronounced peaks in the experimental spectrum.

In macromolecular X-ray crystallography, cryocooling techniques are typically utilized to help minimize radiation damage to the crystal with an ensuing loss of high-resolution diffraction patterns. However, with the high intensity of third-generation synchrotrons, radiation damage occurs even at cryotemperatures (*47*). An X-ray dose of 20 MGy (Gy = $J \cdot kg^{-1}$) for cryocooled (77 K) protein crystals was determined by Henderson to result in a 50% reduction in diffraction intensity and has been the benchmark radiation dose used for protein crystallography studies (*34*). Note that Henderson's conclusions were derived from the results of e-beam diffraction experiments (*34*). Recently, these conclusions were confirmed from the results of experiments on several protein crystals using third-generation X-ray synchrotron sources (*47*).

The radiation-induced radical concentration at low temperature saturates. This saturation behavior can be accounted for by an increase of radical recombination rate with an increase in radical concentration. We have followed the generation of radicals after different doses of radiation and observe that half-saturation of the formation of radiation-induced radicals occurred at 0.6 MGy at 77 K (Figure 2). No degradation of the crystal shape was observed by visible

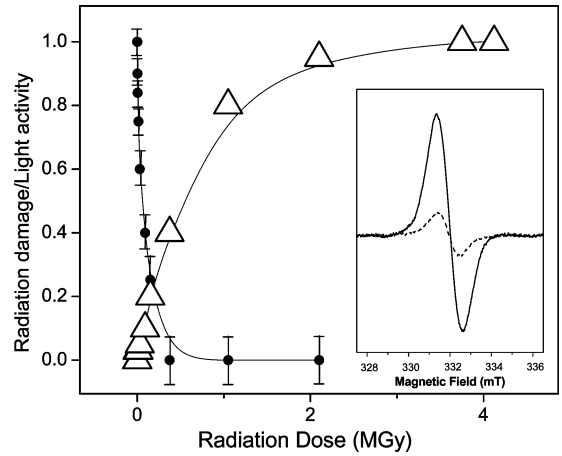

FIGURE 2: Normalized amplitudes of light-induced protein electron transfer activity (circles with bars) and radical accumulation (triangles) plotted as a function of radiation dose. The electron transfer activity of the RC was measured as the intensity of the light-induced spectrum of the charge-separated state $P^+Q_A^-$ measured by continuous illumination of the RC crystal in the X-band EPR cavity at 4 K (insert, solid line; crystal was irradiated with a 4.5 kGy dose) minus the spectrum recorded in the dark (insert, dashed line). Errors in the signal amplitude measurements are indicated with bars. Radical accumulation was measured by double integration of X-band EPR spectra recorded as a first derivative of the absorption. Irradiation of the crystal was carried out at 77 K.

inspection following a saturating dose of radiation; the crystal remained intact. The color of the crystal, however, became darkened and changed completely from dark blue to black at doses higher than 0.2 MGy. Importantly, the dosage at which we observe saturation of radiation damage, i.e., radical formation, is more than 1 order of magnitude smaller than the typical dose of radiation at which protein crystals have been reported to lose their diffraction quality. The D-parameters are conserved at each radiation dose (see Figure 1A), and hence, the distances between the radical pairs do not change as the dose is increased and saturation occurs. This observation confirms that a uniform protein structure within the crystal is still conserved at doses that correspond to saturation of radical formation. Our profile of the formation of radicals is similar to the X-ray dose profile of damage to the active metal site of PSII (*7*). Mn(II) content was used to measure radiation damage to the oxygen evolving Mn_4Ca complex in PSII, and similar to our EPR results, the damage occurred at 1 order of magnitude lower than the dose that is commonly considered safe for protein crystallography.

Prior to radiation exposure, the activity of RC single crystals can be observed as the light-induced appearance of the charge-separated state $P^+Q_A^-$ in the X-band EPR spectrum at low temperature. The amplitude of the light-induced $P^+Q_A^-$ signal was used to assay the extent of photosynthetic activity of RC single crystals and is shown plotted as a function of radiation dose in Figure 2. Surprisingly, RC light-induced activity was found to decay by half after irradiation with a relatively low dose, 50 kGy (Figure 2). This dose, at which light-induced RC activity in the crystalline environment decayed, is an order of magnitude lower than the 0.6 MGy dose at which half-saturation of radiation-induced radicals is observed and approximately 2 orders of magnitude lower than the dosage typically used for protein crystallography (*34, 47*), i.e., presumably comparable to doses required for RC structure determination

(*9, 16*−*21*). In addition, we note that a light-induced EPR signal of the triplet state of the primary electron donor bacteriochlorophyll special pair was not observed in the inactivated samples. This triplet state is normally generated by recombination of the radical pair P^+H^-, where H is the primary bacteriopheophytin electron acceptor, when forward electron transfer from H to to Q_A is blocked, e.g., by quinone extraction or quinone reduction prior to photoexcitation (*48*). The absence of a P-triplet EPR signal suggests that e-beam irradiation modifies the RCs at the level of the primary donor, i.e., special pair, P, and bacteriopheophytin, H, such that triplet cannot form. These results indicate that both the primary charge separation and sequential transfer to the quinone acceptors are blocked following remarkably low levels of radiation exposure. To determine whether or not crystals regain light-induced activity after annealing, we warmed two e-beam irradiated crystals to $T = 273$ K. One crystal had been irradiated with a dose of 0.15 MGy, the second with a dose of 0.375 MGy. Both crystals regained their photochemical activity after warming, as evidenced by the light-induced EPR signal of $P^+Q_A^-$ observed at 4 K. In contrast, two crystals that were irradiated with doses higher than 1 MGy did not regain any light-induced activity after warming to $T = 273$ K. Thus, RCs irradiated with higher doses are irreversibly damaged by the radiation and nonfunctional.

Accordingly, we can discern two mechanisms for radiation-induced inactivation of RCs. The first is a reversible inactivation that occurs at radiation doses below 1 MGy and presumably either involves the reversible formation of trapped free radical states on protein sites that quench early light-induced excited states or involves the direct reduction/oxidation of the cofactors and consequential interruption of normal light-induced electron transfer. The second mechanism is an irreversible inactivation that occurs at radiation doses above 1 MGy and presumably is linked to irreversible critical bond breakage.

Evidence for Radiation-Induced Quinone Reduction. Evidence for the radiation-induced reduction of quinone cofactors can be demonstrated by HF D-band EPR measurements following temperature warming protocols. Radiation exposure leads to the creation of a high concentration of different radicals and radical pairs whose EPR signals overwhelm EPR signals from reduced/oxidized RC cofactors. Radical pair EPR signals and shallowly trapped free radicals can be removed by sample annealing at temperatures around the glass transition (*42, 43*) The quinone sites, the final electron acceptors in the RC, could act as electron "sinks" where the radiation-induced photoelectrons are more stably trapped.

We observed substantial attenuation of low-temperature EPR signals in irradiated crystal after warming to 190 K. Figure 3 shows a resulting D-band spectrum for a crystal having received a 0.3 MGy dose. A residual signal persists after annealing to temperatures up to 260 K. The positions of the *g*-tensor resolved low-field peaks of the HF EPR signal in the 4.6360−4.6380 T range are very specific for reduced quinones (*25*). Thus, we assign the low-field signals as radiation-induced quinone anion radicals. This assignment can be confirmed by comparison of the radiation-induced spectrum to light-induced $P^+Q_A^-$ HF EPR signals in Fe-removed/Zn-replaced RC, also shown in Figure 3. Residual free radical signals distinct from the quinone signals are observed at higher field. The *g*-values of these signals are

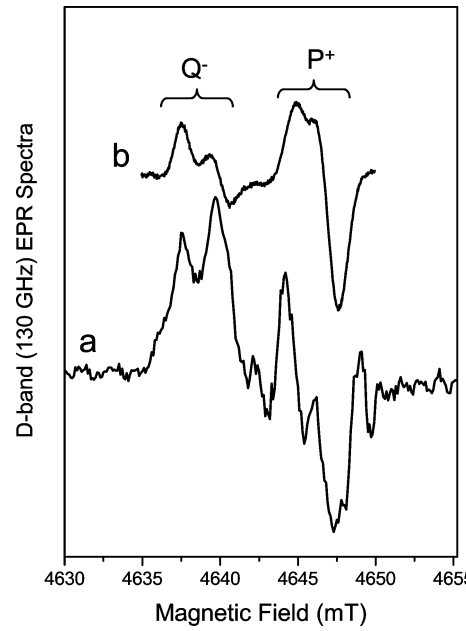

FIGURE 3: (a) High-field D-band (130 GHz) EPR spectrum of the RC protein crystal recorded at 10 K after e-beam irradiation with a 0.3 MGy dose at 77 K and 20 min annealing at 190 K. A background signal from the radiation-induced paramagnetic center in quartz was subtracted. (b) D-band (130 GHz) EPR spectrum of the charge-separated state $P^+Q_A^-$ recorded in a RC solution. The distinct spectral regions where the reduced quinone acceptors Q_A^- and Q_B^- and oxidized primary donor P^+ contribute are indicated on top. Note, the *g*-value of the primary donor P^+ is close to the *g*-value of the free electron. In this region, numerous organic radicals have appreciable EPR intensities. For this reason, the signal from the irradiated crystal in this region cannot be directly assigned to P^+.

consistent with the *g*-values of bacteriochlorophyll and bacteriopheophytin radical ions. However, the *g*-values of these cofactor signals are close to the free electron *g*-value, and numerous organic radicals (for example, residual amino acid radicals that have not annealed) could contribute to the observed signals in this spectral region. Thus, we are unable to differentiate and identify these radicals. Importantly, however, HF EPR provides direct evidence for the presence of reduced quinone cofactors at low dose radiation exposure of RC single crystals.

Implications for RC Crystal Structure Interpretation. EPR experiments show that the formation of radiation-induced free radicals saturated at doses 1 order of magnitude smaller than the amount of radiation at which protein crystals lose their diffraction quality, while light-induced RC activity was found to be lost at radiation doses at least 1 order of magnitude lower than the dose at which radiation-induced radicals exhibited saturation. These results suggest that substantial radiation-induced modification of crystals occurs during X-ray diffraction data collection and that the resultant 3D X-ray structure does not reflect the native state of the RC, but rather a state inactive to electron transfer. Our results show that the RC crystal structures must be considered as structures containing reduced quinone cofactors and possibly altered redox states on the bacteriochlorophyll and bacteriopheophytin acceptors as well. Consequences of radiation-induced changes in cofactor redox states can be expected to be the most significant for X-ray structures determined at temperatures above the RC "glass transition" (>150 K) that allows conformational relaxation to occur in response to charge formation (*49*−*54*). While a large-scale movement

of cofactors or side chains is not probable at low temperature, some small-scale cofactor reorientation and displacement due to a change in redox state (*35, 55*) as well as localized peptide disorder from site-specific radiation damage (*47*) might happen even at low temperatures. Ultimately, our data suggest that multiplicities seen in the Q_B binding site in the various bacterial RC crystal structures (*16, 17, 19, 20, 32, 56, 57*) may result in part from radiation-induced variations in Q_B reduction and protonation states.

In summary, EPR measurements show that a substantial amount of radical formation occurs in RC crystals, and this radiation damage happens at much lower doses than were predicted to be a problem by the qualitative loss of diffraction intensity. Thus, the dose safe for data collection of redox-active proteins is lower than previously thought (*34, 47*), as recently reported (*7*). A suite of spectroscopic and molecular biology techniques, in addition to X-ray crystallography, are necessary to truly delineate specific structure−function relationships of the dynamic light-induced electron transfer reactions in RC proteins.

REFERENCES

1. Chance, B., Angiolillo, P., Yang, E. K., and Powers, L. (1980) Identification and assay of synchrotron radiation induced alterations on metalloenzymes and proteins. *FEBS Lett. 112*, 178–182.
2. Weik, M., Ravelli, R. B. G., Kryger, G., McSweeney, S., Raves, M. L., Harel, M., Gros, P., Silman, I., Kroon, J., and Sussman, J. L. (2000) Specific chemical and structural damage to proteins produced by synchrotron radiation. *Proc. Natl. Acad. Sci. U.S.A. 97*, 623–628.
3. Wuerges, J., Lee, J.-W., Yim, Y.-I., Yim, H.-S., Kang, S.-O., and Carugo, K. D. (2004) Crystal structure of nickel-containing superoxide dismutase reveals another type of active site. *Proc. Natl. Acad. Sci. U.S.A. 101*, 8569–8574.
4. Carugo, O., and Carugo, K. D. (2005) When X-rays modify the protein structure: radiation damage at work. *Trends Biochem. Sci. 30*, 213–219.
5. Garman, E. F., and McSweeney, S. M. (2007) Progress in research into radiation damage in cryo-cooled macromolecular crystals. *J. Synchrotron Rad. 14*, 1–3.
6. Pearson, A. R., Pahl, R., Kovaleva, E. G., Davidson, V. L., and Wilmot, C. M. (2007) Tracking X-ray-derived redox changes in crystals of a methylamine dehydrogenase/amicyanin complex using single-crystal UV/Vis microspectrophotometry. *J. Synchrotron Rad. 14*, 92–98.
7. Yano, J., Kern, J., Irrgang, K.-D., Latimer, M., Bergmann, U., Glatzel, P., Pushkar, Y. N., Biesiadka, J., Loll, B., Sauer, K., Messinger, J., Zouni, A., and Yachandra, V. K. (2005) X-ray damage to the Mn_4Ca complex in single crystals of photosystem II: A case study for metalloprotein crystallography. *Proc. Natl. Acad. Sci. U.S.A. 102*, 12047–12052.
8. Deisenhofer, J., Epp, O., Miki, K., Huber, R., and Michel, H. (1984) X-ray structure analysis of a membrane protein complex: electron density map at 3 Å resolution and a model of the chromophores of the photosynthetic reaction center from *Rhodopseudomonas viridis*. *J. Mol. Biol. 180*, 385–398.
9. Ermler, U., Fritzsch, G., Buchanan, S., and Michel, H. (1994) Structure of the photosynthetic reaction-center from *Rhodobacter sphaeroides* at 2.65 Angstrom resolution−cofactors and protein-cofactor interactions. *Structure 2*, 925–936.
10. Parson, W. W. (1987) The bacterial reaction center, in *Photosynthesis* (Amesz, J., Ed.) pp 43−61, Elsevier, New York.
11. Feher, G., Allen, J. P., Okamura, M. Y., and Rees, D. C. (1989) Structure and function of bacterial photosynthetic reaction centers. *Nature 339*, 111–116.
12. Okamura, M. Y., Paddock, M. L., Graige, M. S., and Feher, G. (2000) Proton and electron transfer in bacterial reaction centers. *Biochim. Biophys. Acta 1458*, 148–163.
13. Mancino, L., Dean, D., and Blankenship, R. (1984) Kinetics and thermodynamics of the $P870^+Q_A^-$−$P870^+Q_B^-$ reaction in isolated reaction centers from the photosynthetic bacterium *Rhodopseudomonas sphaeroides*. *Biochim. Biophys. Acta 764*, 46–54.
14. Tiede, D. M., Vazquez, J., Cordova, J., and Marone, P. A. (1996) Time-resolved electrochromism associated with the formation of quinone anions in the *Rhodobacter sphaeroides* R26 reaction center. *Biochemistry 35*, 10763–10775.
15. Graige, M. S., Feher, G., and Okamura, M. Y. (1998) Conformational gating of the electron transfer reaction $Q_A^-Q_B$−$Q_AQ_B^-$ in bacterial reaction centers of *Rhodobacter sphaeroides* determined by a driving force assay. *Proc. Natl. Acad. Sci. U.S.A. 95*, 11679–11684.
16. Stowell, M. H. B., McPhillips, T. M., Rees, D. C., Soltis, S. M., Abresch, E., and Feher, G. (1997) Light-induced structural changes in photosynthetic reaction center: Implications for mechanism of electron-proton transfer. *Science 276*, 812–816.
17. Kuglstatter, A., Ermler, U., Michel, H., Baciou, L., and Fritzsch, G. (2001) X-ray structure analyses of photosynthetic reaction center variants from *Rhodobacter sphaeroides*: Structural changes induced by point mutations at position L209 modulate electron and proton transfer. *Biochemistry 40*, 4253–4260.
18. Fritzsch, G., Koepke, J., Diem, R., Kuglstatter, A., and Baciou, L. (2002) Charge separation induces conformational changes in the photosynthetic reaction centre of purple bacteria. *Acta Crystallogr. D58*, 1660–1663.
19. Pokkuluri, P. R., Laible, P. D., Crawford, A. E., Mayfield, J. F., Yousef, M. A., Ginell, S. L., Hanson, D. K., and Schiffer, M. (2004) Temperature and cryoprotectant influence secondary quinone binding position in bacterial reaction centers. *FEBS Lett. 570*, 171–174.
20. Baxter, R. H. G., Seagle, B.-L., Ponomarenko, N., and Norris, J. (2004) Specific radiation damage illustrates light-induced structural changes in the photosynthetic reaction center. *J. Am. Chem. Soc. 126*, 16728–16729.
21. Koepke, J., Krammer, E.-M., Klingen, A. R., Sebban, P., Ullmann, G. M., and Fritzsch, G. (2007) pH modulates the quinone position in the photosynthetic reaction center from *Rhodobacter sphaeroides* in the neutral and charge separated states. *J. Mol. Biol. 371*, 396–409.
22. Xu, Q., and Gunner, M. R. (2002) Exploring the energy profile of the Q_A^- to Q_B electron transfer reaction in bacterial photosynthetic reaction centers: pH dependence of the conformational gating step. *Biochemistry 41*, 2694–2701.
23. Breton, J., Boullais, C., Mioskowski, C., Sebban, P., Baciou, L., and Nabedryk, E. (2002) Vibrational spectroscopy favors a unique Q_B binding site at the proximal position in wild-type reaction centers and in the Pro-L209-Tyr mutant from *Rhodobacter sphaeroides*. *Biochemistry 41*, 12921–12927.
24. Nabedryk, E., Breton, J., Sebban, P., and Baciou, L. (2003) Quinone (Q_B) binding site and protein structural changes in photosynthetic reaction center mutants at Pro-L209 revealed by vibrational spectroscopy. *Biochemistry 42*, 5819–5827.
25. Utschig, L. M., Thurnauer, M. C., Tiede, D. M., and Poluektov, O. G. (2005) Low-temperature interquinone electron transfer in photosynthetic reaction centers from *Rhodobacter sphaeroides* and *Blastochloris viridis*: Characterization of Q_B^- states by high-frequency electron paramagnetic resonance (EPR) and electron-nuclear double resonance (ENDOR). *Biochemistry 44*, 14131–14142.
26. Heinen, U., Utschig, L. M., Poluektov, O. G., Link, G., Ohmes, E., and Kothe, G. (2007) Structure of the charge separated state $P^+Q_A^-$ in the photosynthetic reaction centers of *Rhodobacter sphaeroides* by quantum beat oscillations and high-field electron paramagnetic resonance: Evidence for light-induced Q_A^- reorientation. *J. Am. Chem. Soc. 129*, 15935–15946.
27. Savitsky, A., Dubinski, A. A., Flores, M., Lubitz, W., and Mobius, K. (2007) Orientation-resolving pulsed electron dipolar high-field EPR spectroscopy on disordered solids: I. Structure of spin-correlated radical pairs in bacterial photosynthetic reaction centers. *J. Phys. Chem. B 111*, 6243–6262.
28. Thurnauer, M. C., Poluektov, O., and Kothe, G. (2004) Time-resolved high frequency and multifrequency EPR studies of spin-correlated radical pairs in photosynthetic reaction center proteins, in *Biological Magnetic Resonance: Very High Frequency (VHF) ESR/EPR* (Grinberg, O. Y., and Berliner, L. J., Eds.) pp 165−206, Kluwer Academics, New York.
29. Mobius, K., Savitsky, A., Schnegg, A., Plato, M., and Fuchs, M. (2005) High-field EPR spectroscopy applied to biological systems: characterization of molecular switches for electron and ion transfer. *Phys. Chem. Chem. Phys. 7*, 19–42.
30. Utschig, L. M., Greenfield, S. R., Tang, J., Laible, P. D., and Thurnauer, M. C. (1997) Influence of iron-removal procedures on

sequential electron transfer in photosynthetic bacterial reaction centers studied by transient EPR spectroscopy. *Biochemistry 36*, 8548–8558.
31. Isaacson, R. A., Lendzian, F., Abresch, E. C., Lubitz, W., and Feher, G. (1995) Electronic structure of Q_A^- in reaction centers from *Rhodobacter sphaeroides*. I. Electron paramagnetic resonance in single crystals. *Biophys. J. 69*, 311–322.
32. Pokkuluri, P. R., Laible, P. D., Deng, Y.-L., Wong, T. N., Hanson, D. K., and Schiffer, M. (2002) The structure of a mutant photosynthetic reaction center shows unexpected changes in main chain orientations and quinone position. *Biochemistry 41*, 5998–6007.
33. Spinks, J. W. T., and Woods, R. J. (1990) *An Introduction to Radiation Chemistry*, John Wiley & Sons, New York.
34. Henderson, R. (1990) Cryoprotection of protein crystals against radiation-damage in electron and x-ray diffraction. *Proc. R. Soc. London, Ser. B 241*, 6–8.
35. Poluektov, O. G., Utschig, L. M., Dubinski, A. A., and Thurnauer, M. C. (2005) Electron transfer pathways and protein response to charge separation in photosynthetic reaction centers: Time-resolved high-field ENDOR of the spin-correlated radical pair $P_{865}^+Q_A^-$. *J. Am. Chem. Soc. 127*, 4049–4059.
36. Kawrakow, I. (2000) Accurate condensed history Monte Carlo simulation of electron transport. I. EGSnrc, the new EGS4 version. *Med. Phys. 27*, 485–498.
37. Luse, R. A. (1964) Basic mechanisms in the radiation chemistry of proteins and the nucleic acids. *Radiat. Res., Suppl. 4*, 192–212.
38. Symons, M. C. (1995) Electron spin resonance studies of radiation damage to DNA and to proteins. *Radiat. Phys. Chem. 45*, 837–845.
39. Burmeister, W. P. (2000) Structural changes in a cryo-cooled protein crystal owing to radiation damage. *Acta Crystallogr. D56*, 328–341.
40. Ravelli, R. B. G., and McSweeney, S. M. (2000) The "fingerprint" that X-rays can leave on structures. *Structure 8*, 315–328.
41. O'Neill, P., Stevens, D. L., and Garman, E. F. (2002) Physical and chemical considerations of damage induced in protein crystals by synchrotron radiation: a radiation chemical perspective. *J. Synchrotron Rad. 9*, 329–332.
42. Zaikov, G. E., and Sharpatyi, V. A. (2006) *Radiation Chemistry of Biopolymers*, Brill, Leiden, The Netherlands.
43. Zubkov, A. V., Koritskii, A. T., and Lebedev, Y. S. (1968) Formation of pairs of radicals during the radiolysis and photolysis of organic peroxides. *Dokl. Akad. Nauk SSSR 180*, 1150–1153.
44. Shiga, T., Lund, A., and Kinell, P.-O. (1971) Electron spin resonance studies of primary processes in radiation-induced reactions. II. Single crystal 1,3-butadiene. *Int. J. Rad. Phys. Chem. 3*, 145–153.
45. Dulcic, A., and Herak, J. N. (1973) Radiation-induced pair-wise radical formation in single crystals of thymine. *Biochim. Biophys. Acta 319*, 109–115.
46. Grinberg, O. Y., and Berliner, L. J. (2004) Very high frequency (VHF) ESR/EPR, in *Biological Magnetic Resonance*, Kluwer Academic, Plenum Publishers, New York.
47. Owen, R. L., Rudino-Pinera, E., and Garman, E. F. (2006) Experimental determination of the radiation dose limit for cryo-cooled protein crystals. *Proc. Natl. Acad. Sci. U.S.A. 103*, 4912–4917.
48. Thurnauer, M. C., Katz, J. J., and Norris, J. R. (1975) The triplet state in bacterial photosynthesis: possible mechanisms of the primary photo-act. *Proc. Natl. Acad. Sci. U.S.A. 72*, 3270–3274.
49. Kleinfeld, D., Okamura, M. Y., and Feher, G. (1984) Electron-transfer kinetics in photosynthetic reaction centers cooled to cryogenic temperatures in the charge-separated state: Evidence for light-induced structural changes. *Biochemistry 23*, 5780–5786.
50. Tiede, D. M., Kellogg, E., and Breton, J. (1987) Conformational changes following reduction of the bacteriopheophytin electron acceptor in reaction center of *Rhodopseudomonas viridis*. *Biochim. Biophys. Acta 892*, 294–302.
51. Tiede, D. M., and Hanson, D. K. (1992) Protein relaxation following quinone reduction in *Rhodobacter capsulatus*: Detection of likely protonation-linked optical absorbance changes of the chromophores, in *The Photosynthetic Bacterial Reaction Center II* (Breton, J., and Vermeglio, A., Eds.) pp 341−350, Academic Press, New York.
52. Muh, F., Williams, J. C., Allen, J. P., and Lubitz, W. A. (1998) A conformational change of the photoactive bacteriopheophytin in reaction centers from *Rhodobacter sphaeroides*. *Biochemistry 37*, 13066–13074.
53. Poluektov, O. G., Utschig, L. M., Dalosto, S., and Thurnauer, M. C. (2003) Probing local dynamics of the photosynthetic bacterial reaction center with a cysteine specific spin label. *J. Phys. Chem. B 107*, 6239–6244.
54. Borovykh, I. V., Gast, P., and Dzuba, S. A. (2005) "Glass transition" near 200 K in the bacterial photosynthetic reaction center protein detected by studying the distances in the transient $P^+Q_A^-$ radical pair. *J. Phys. Chem. B 109*, 7535–7539.
55. Faller, P., Goussias, C., Rutherford, A. W., and Un, S. (2003) Resolving intermediates in biological proton-coupled electron transfer: a tyrosyl radical prior to proton movement. *Proc. Natl. Acad. Sci. U.S.A. 100*, 8732–8735.
56. Lancaster, C. R. (1999) Quinone-binding sites in membrane proteins: What can we learn from the *Rhodopseudomonas viridis* reaction centre? *Biochem. Soc. Trans. 27*, 591–596.
57. Baxter, R. H. G., Seagle, B.-L., Ponomarenko, N., and Norris, J. (2005) Cryogenic structure of the photosynthetic reaction center of *Blastochloris viridis* in the light and dark. *Acta Crystallogr. D61*, 605–612.

BI800574E